Investigation of Thermal Dispersion and Thermally-Induced Birefringence on High-Power Double Clad Yb:Glass Fiber Laser

M. Sabaeian[a] and H. Nadgaran[b]
[a]Department of Physics, Shahid Chamran University of Ahwaz, Ahwaz, Iran
[b]Department of Physics, Shiraz University, Shiraz 71454, Iran.

Abstract— **In this work the effects of heat generation on the modes of Yb:Glass double clad fiber laser were investigated. The thermal dispersion and thermally-induced birefringence were considered when the gain medium becomes an anisotropic medium. The results showed considerable modifications of laser modes profiles, in particular for transfer magnetic (TM) and transfer electric (TE) modes which their polarization vectors possess radial and azimuthal components.**

KEYWORDS: Birefringence, Fiber laser, Thermal dispersion, Thermal effects, Thermally-induced stress.

I. INTRODUCTION

Yb^{3+}-doped silica double clad fiber lasers are considered suitable for high power operation because of broad absorption band and strong absorption and emission cross section of Ytterbium ions. Although features like a large surface to volume ratio and a high quantum efficiency together with long length seems to prevent heat accumulation inside the fibers and make the heat flow simpler, recent developments in escalated power fiber lasers [1], however have led to typical thermal loadings of about $35W/m$ or more, which can have dramatic effects on lasers operation [1], [2]. Worth to name several mechanisms responsible for heat generation: non-unity of quantum efficiency of pump level and the laser meta-stable state, concentration quenching and energy up-conversion [3].

In addition to the overall temperature increase that might cause damage of fiber polymer coatings or degrade laser efficiency by thermally populating the lower laser level [4], the induced temperature gradient leads to a number of effects such as thermal dispersion or dn/dT effect and birefringence due to thermally-induced stresses (strains).

Although there are many works on temperature modeling for fiber laser media [5]-[10], one can hardly find works on mode characteristics based on the direct solution of the wave equation in the medium. Among them the work of Hardrich *et al.* [5] showed that thermal lensing can convert single-mode photonic crystal fiber lasers to multimode one due to excitation of frozen modes. Also, the work of Sabaeian *et al.* [6] considered the thermal lensing effect on mode deformations and core and cladding confinement factor (CCF) variations in an octagonal double clad fiber laser where their simulation revealed a dramatic change in CCF for preliminary mode families. CCF factor is a measure of deviation of modes from their standard shapes. In those works the thermal lensing has merely been taken into account and the other thermal effects such as the induced birefringence, was ignored. Here for the first time, the thermally-induced birefringence was also taken into account to present a comprehensive study on the core and cladding modes shapes and polarization variations. Induced birefringence in initially isotropic medium is a direct consequence of thermal strains (stresses). As a result, the refractive indices in three perpendicular directions (n_x, n_y, n_z) becomes unequal. Here, in this work the uniform change of refractive index due to thermal lensing or thermal dispersion plus anisotropic changes due to

thermally-induced birefringence are all included in the wave equation, and eigenmodes of core and cladding are simulated by numerical method of finite element. The results show a noticeable change in modes' shape and in particular demolishing of some of the useful polarization components. This of course has undesirable effects on beam quality as well as pump efficiency. This demolishing of some polarization components due to thermal effects might seldom produce a single-mode single-component polarization fiber laser out of a multi-component polarization fiber [11].

In this work we first solve the heat equation to find the temperature distribution inside the fiber. A uniform source is considered to shine the fiber core where the active Yb^{+3} ions exist. Heat radiations as well as heat convection were both considered for a complete set of boundary conditions. This heat radiation which always exists, especially in high heat load, was usually ignored in previous works to simplify the models [9], [10] and [12]. Then, variations of the medium refractive index due to thermal dispersion and thermal stresses are calculated. Finally, the wave equation with modified refractive index will be solved and eigenmodes will be simulated.

II. TEMPERATURE DISTRIBUTION AND REFRACTIVE INDEX VARIATIONS

For modeling the temperature distribution and changes of refractive index, we consider a double clad fiber in which the central region of radius a contains active ions of Yb^{+}. The inner cladding of radius b and outer cladding of radius c contain no additional doping and so they do not have any contribution to heat source. For a long length fiber laser, one can ignore the variation of temperature along the fiber as a good approximation [7]-[10]. So, the heat equation can be written as follows [6]:

$$\begin{aligned} &\frac{\partial^2 T}{\partial r^2}+\frac{1}{r}\frac{\partial T}{\partial r}=-\frac{P_h}{\pi a^2 K_s} && r\le a \\ &\frac{\partial^2 T}{\partial r^2}+\frac{1}{r}\frac{\partial T}{\partial r}=0 && a<r\le c \end{aligned} \qquad (1)$$

where P_h is the heat load power per unit length and K_s is the silica thermal conductivity. The heat generated in the core flows toward boundaries via conduction then exchange with the ambient via convection and radiation processes. This can be written as [6], [12]:

$$K_a \frac{\partial T}{\partial r}\Big|_{r=c}+h\left(T-T_\infty\right)\Big|_{r=c}+\varepsilon\sigma_{SB}\left(T^4-T_s^4\right)\Big|_{r=c}=0 \qquad (2)$$

where K_a is the polymer thermal conductivity, h is the heat transfer coefficient, ε is the fiber surface emissivity and σ_{SB} is Stefan-Boltzman constant. T_∞ and T_s are the fluid temperature at the very far and the ambient temperature, respectively. For the most cases, these two are the same. For the inner boundaries, the continuity of the temperature function over the core and inner cladding together with the continuity of its normal derivatives form a set of boundary conditions.

In the absence of the radiation term in Eq.(2), the following analytical solutions can be obtained for the three different regions of the fiber laser:

$$\begin{aligned} T_1(r)&=T_0-\frac{P_h r^2}{4\pi a^2 K_s} && 0\le r\le a \\ T_2(r)&=T_0-\frac{P_h}{4\pi K_s}\left(1+\ln\left(\frac{r}{a}\right)\right) && a\le r\le c \end{aligned} \qquad (3)$$

where

$$T_0=T_s+\frac{Q_0 a^2}{4K_s}\left[1+2\ln\left(\frac{c}{a}\right)+\frac{2K_a}{hc}\right] \qquad (4)$$

shows the core center temperature. In the case where the radiation term is included in Eq. (2), the analytical solution to the heat equation can no longer be found easily and we have to use a numerical method. Before proceeding further, it is crucial to show that the radiation term plays a very important role in such models and its usual ignorance in the literature can not be justified at least when we are facing a high heat load. Fig.(1) shows the temperature of the center of the core against the heat load per fiber length for the two cases mentioned above. It is very much clear from the figure that at the low heat load, the two solutions, namely with and without the radiation term, are almost the same. As heat load is increasing, however the difference between the two cases is noticeable

confirming that the radiation term should be taken into account in most thermal models.

Figure (2) obviously shows a pronounced temperature gradient for three different amount of heat load per unit length. Nowadays cooling mechanisms have been improved, but this temperature gradient is still induced across the fiber and is mainly responsible for thermal effects.

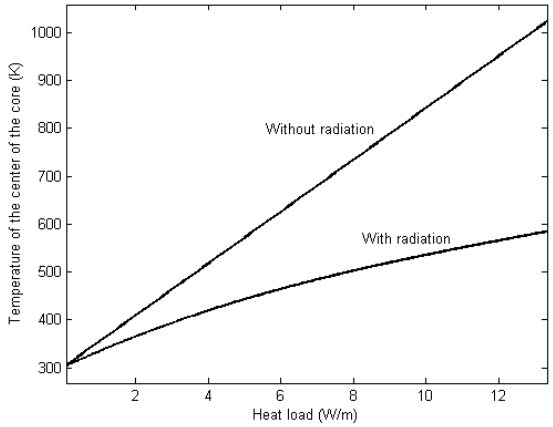

Fig. 1 Temperature of the center of the core versus heat load with and without considering radiation from the boundary.

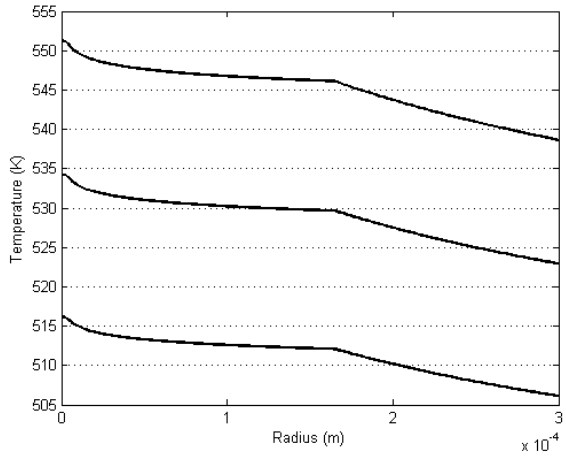

Fig. 2 Temperature distribution versus the fiber radius for three values of heat load, from the top to the down for $P_h = 50$, 45 and $40 W/m$, respectively.

The modified refractive indices of the gain medium due to non-uniform temperature distribution are then given as [14]:

$$n_{xx} = n_0 + \left(\frac{\partial n}{\partial T}\right)(T - T_s) - B_{\perp}\sigma_{zz} - B_{\parallel}\sigma_{xx} \quad (5)$$

$$n_{yy} = n_0 + \left(\frac{\partial n}{\partial T}\right)(T - T_s) - B_{\perp}(\sigma_{zz} + \sigma_{xx}) \quad (6)$$

$$n_{zz} = n_0 + \left(\frac{\partial n}{\partial T}\right)(T - T_s) - B_{\perp}\sigma_{xx} - B_{\parallel}\sigma_{zz} \quad (7)$$

where the first terms are the refractive index at ambient temperature, the second terms shows uniform variations for the refractive index and remaining terms induce anisotropic variations for the refractive index leading to the medium birefringence. $B_{\perp}$ and $B_{\parallel}$ are perpendicular and parallel elasto-optic coefficients, respectively. σ_{xx}, σ_{yy} and σ_{zz} are the stress components related to the strain components ε_{ij} via [15]:

$$\sigma_{xx} = \frac{E}{1-\nu^2}\left[(1-\nu)\varepsilon_{xx} + \nu\,\varepsilon_{yy} + \nu\,\varepsilon_{zz}\right] \quad (8)$$

$$\sigma_{yy} = \frac{E}{1-\nu^2}\left[\nu\varepsilon_{xx} + (1-\nu)\,\varepsilon_{yy} + \nu\,\varepsilon_{zz}\right] \quad (9)$$

$$\sigma_{zz} = \frac{E}{1-\nu^2}\left[\nu\varepsilon_{xx} + \nu\,\varepsilon_{yy} + (1-\nu)\,\varepsilon_{zz}\right] \quad (10)$$

where ν is the Poisson ratio and E is the Young modulus. The induced strains are the result of the temperature gradient inside the medium. The equation describing this effect is given as [16]:

$$\frac{1-\nu}{1+\nu}\vec{\nabla}\left(\vec{\nabla}\cdot\vec{u}\right) - \frac{1-2\nu}{1+\nu}\vec{\nabla}\times\vec{\nabla}\times\vec{u} = \alpha_T\vec{\nabla}T \quad (11)$$

where α_T is the thermal expansion coefficient and $\vec{u}$ is the displacement vector where its components are related to the strain components as:

$$\varepsilon_{ij} = \frac{1}{2}\left(\frac{\partial u_i}{\partial x_j} + \frac{\partial u_j}{\partial x_i}\right) \quad (12)$$

By solving Eq. (11) in plane strain approximation regime, one can extract the strain components as [6]:

$$\varepsilon_{xx} = \varepsilon_{yy} = \frac{(\nu^2 - 1)}{20\nu^2 - 14\nu + 2}\alpha_T(T - T_s) \quad (13)$$

$$\varepsilon_{zz} = \frac{2(3\nu - 1)(\nu + 1)}{20\nu^2 - 14\nu + 2}\alpha_T(T - T_s) \quad (14)$$

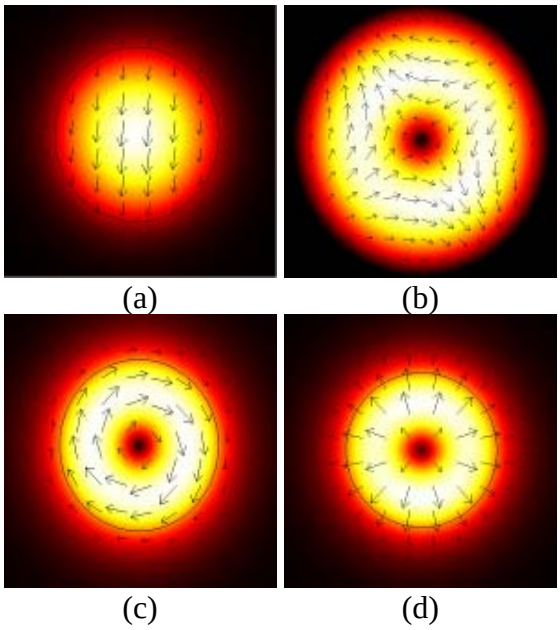

Fig. 3. Electric field profile of HE_{11} (a), EH_{21} (b), TE_{01} (c) and TM_{01} (d) modes of the core for $P_h=0$.

In deriving the above expressions we assumed that the mechanical properties of three regions of the fiber laser are the same [6], [9] and [10].

III. WAVE EQUATION IN INHOMOGENEOUS AND ANISOTROPIC MEDIA

Using Maxwell equations, the wave equation for an inhomogeneous and anisotropic medium, takes the form of:

$$\vec{\nabla}\times\vec{\nabla}\times\vec{\mathrm{E}}(\vec{r},t)+\frac{n^2(\vec{r})}{c^2}\vec{\mathrm{E}}(\vec{r},t)=0 \qquad (15)$$

where n is the refractive index tensor and can be written as

$$n=\begin{pmatrix} n_{xx} & 0 & 0 \\ 0 & n_{yy} & 0 \\ 0 & 0 & n_{zz} \end{pmatrix} \qquad (16)$$

and its component have been given in Eqs.(5)-(7). Assuming a solution of:

$$\vec{E}_{mn}(\vec{r})=\vec{E}_0\,\psi_{mn}(x,y)e^{i\beta_{mn}z}\,e^{-i\omega t} \qquad (17)$$

where $\psi_{mn}(x,y)$ is the electric field profile, β_{mn} is the propagation constant and m and n refer to the azimuthal and radial coordinates, and inserting this solution into Eq.(15), we end up with:

$$\nabla^2\vec{E}'(\vec{r})+\frac{n^2(\vec{r})\omega^2}{c^2}\vec{E}'(\vec{r})=-\vec{\nabla}\left(\frac{\vec{\nabla}n^2(\vec{r})}{n^2(\vec{r})}\cdot\vec{E}'(\vec{r})\right) \qquad (18)$$

where $\vec{E}'_{mn}(\vec{r})=\vec{E}_0\,\psi_{mn}(x,y)e^{i\beta_{mn}z}$ is the spatial part of the propagating wave. The simultaneous solutions for the transverse and longitudinal components of electric field were obtained by finite element method (FEM) in which a very fine grain meshes were used. The core, for example, was divided into 1×10^7 meshes, that is the number of meshes was so high that reliable numerical calculations were achieved. In this respect the mesh curvature cut-off that is a measure of prevention of the generation of many elements around small curved part of the geometry was assumed to be as low as 0.001.

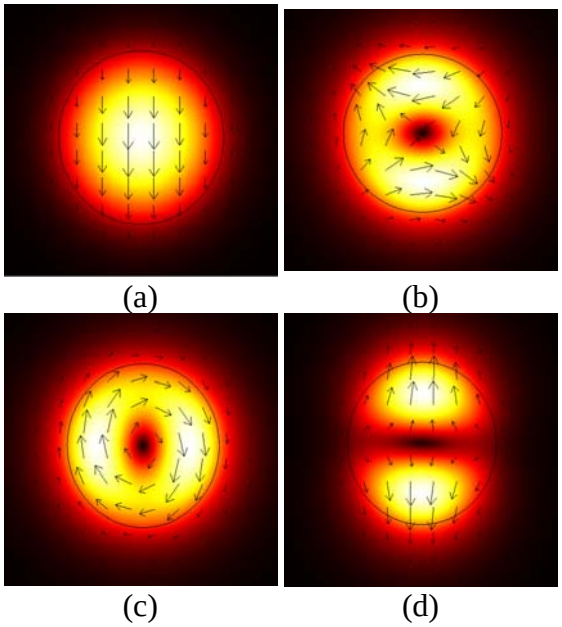

Fig. 4 Electric field profile of HE_{11} (a), EH_{21} (b), TE_{01} (c) and TM_{01} (d) modes of the core for $P_h=10$ W/m.

In making the simulations, the following boundary conditions were also employed:

1) Continuity of the electric field vector on the core-inner clad boundaries.

2) A perfect electric conductor is assumed for the inner clad-outer clad boundaries, i.e.

$\hat{n} \times \vec{E} = 0$, where $\hat{n}$ is the outward unit vector normal to the boundary surface.

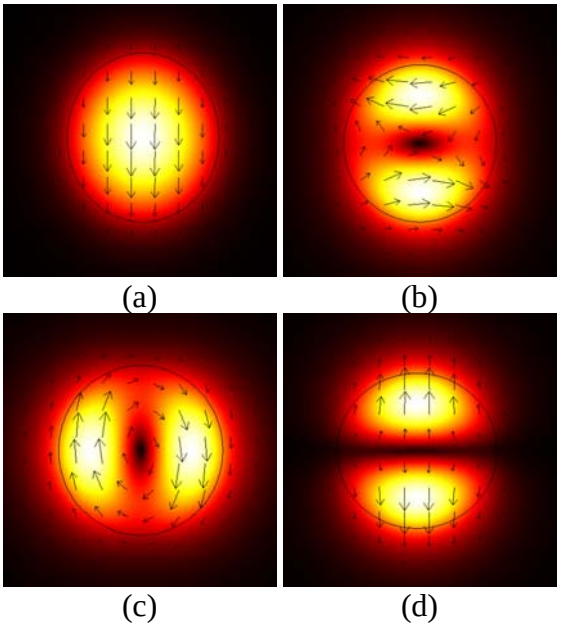

Fig. 5 Electric field profile of HE_{11} (a), EH_{21} (b), TE_{01} (c) and TM_{01} (d) modes of the core for P_h=*40* W/m.

The results of modeling have been used for a cylindrical Yb:Glass double clad fiber laser with $a = 4.8\,\mu m$, $b = 165\,\mu m$ and $c = 300\,\mu m$ [6]. The thermal and mechanical properties of the core and inner cladding are the same. The refractive indices of three regions are $n_1 = 1.4646$, $n_2 = 1.4572$ and $n_3 = 1.3827$, where 1, 2 and 3 refer to the core, inner cladding and outer cladding, respectively [6]. Also, the values of $K_s = 1.38\,Wm^{-1}K^{-1}$ was set for silica core and inner cladding and $K_a = 0.14\,Wm^{-1}K^{-1}$ for polymer outer cladding. Heat transfer coefficient value is $h = 10\,Wm^{-2}K^{-1}$. The variation of refractive index with temperature is $\partial n / \partial T = 1 \times 10^{-5}\,K^{-1}$. The other physical parameters are: $\alpha_T = 0.51 \times 10^{-6}\,K^{-1}$ for thermal expansion coefficient, $E = 7.3 \times 10^{8}\,Kg\,m^{-2}$ for Young modulus and $\nu = 0.16$ for Poisson ratio. The perpendicular and parallel elasto-optic coefficients are $B_{\perp} = 2.27 \times 10^{-11}\,m^2 Kg$ and $B_{\parallel} = 2.27 \times 10^{-11}\,m^2 Kg$. The pump and laser wavelengths are: $\lambda_l = 1120\,nm$ and $\lambda_p = 915\,nm$ [10]. Figure (3) shows the profiles of the core modes for $P_h = 0$, i.e without thermal effects. The influence of heat load on the core modes can be seen in Figs.(4) and (5) for $P_h = 10\,Wm^{-1}$ and $P_h = 40\,Wm^{-1}$, respectively. As it is seen, the fundamental core mode (HE_{11} mode) is hardly affected by the heat load. Instead, the other modes, especially the TE_{01} and TM_{01} modes have experienced the most modifications. Moreover, one of the polarization component of TM_{01} mode has been wiped out.

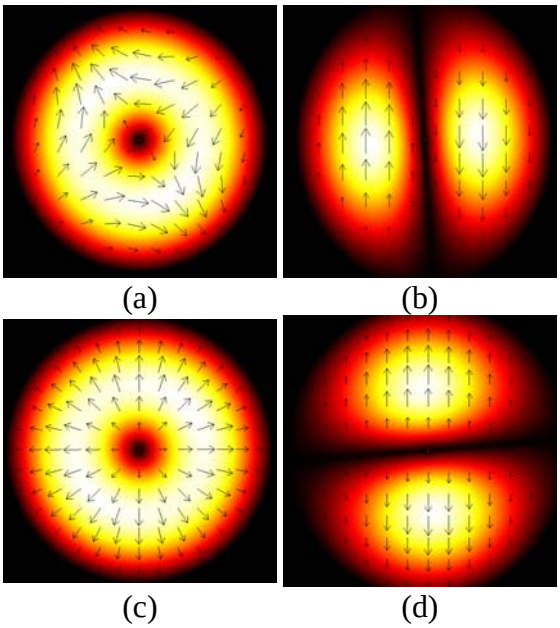

Fig. 6 Electric field profile of HE_{21} mode for P_h=0 (a) and for P_h=10 W/m (b). Also, TM_{01} mode for P_h=0 (c) and for P_h=10 W/m (d).

Figure (6) shows two inner cladding modes, EH_{21} and TM_{01}, at pump wavelength for $P_h = 0$ and $P_h = 10\,Wm^{-1}$. Here also one can see the effects of heat generation on the inner clad propagating modes. Here, too the horizontal component of the polarization has been demolished.

The phenomena observed in Figs. (3) to (5) confirm that the heat generated inside the fiber medium has a dramatic effect on the profile of the propagating modes. These effects can be

interpreted as follows: as the heat generates inside the medium, the thermally-induced stresses due to inhomogeneous temperature distribution converts the optically isotropic glassy medium to an anisotropic one ascertaining the medium birefringence. Then upon electric field passage through the medium, its orthogonal components face different refractive indices.

The cladding modes modifications actually affect the pump efficiency since they deviate from their standard shapes. Furthermore, these core modes alterations under the heat load can have sever impact on the beam quality which is the subject of our further studies.

IV. CONCLUSION

In this work for the first time, we have not only investigated the thermal lensing and its effects on the propagation modes of fiber lasers, but also we have simultaneously included the thermally-induced birefringence effect into our model. An important point is that we have done it by direct addition of these effects into the wave equation. The solution of this type of wave equation was used to simulate the core and inner cladding modes suffered from the induced heat. The results were applied to a double clad Yb:Glass fiber laser with cylindrical symmetry. The simulation results show a considerable modification for the TM and TE propagating modes of the fiber. One interesting results show the demolition of various polarization components too.

In conclusion, thermal effects can seriously modify an isotropic gain medium to an anisotropic one in the sense that the core and the inner clad propagating modes get considerable differences compared to a so called non- thermal fiber laser.

REFERENCES

[1] Y. Wang, "Thermal effects in kilowatt fiber lasers," *IEEE Photon. Tech. Lett.* Vol. 16, pp. 63-65, Jan. 2004.

[2] Y. Jeong, J. K. Sahu, D. N. Payne, and J. Nilsson, "Ytterbium-doped large-core fiber laser with 1.36 kW of continuous-wave output power," *Opt. Express*, Vol. 12, pp. 6088-60921, Oct. 2004.

[3] D. C. Brown, "Heat, Fluorescence, and Stimulated-Emission Power Densities and Fractions in Nd:YAG." *IEEE J. Quantum Electron.*, Vol. 34, pp. 560-572, Mar. 1998.

[4] M. K. Davis and M. J. F. Digonnet, "Measurements of thermal effects in fibers doped with cobalt and vanadium," *IEEE J. Lightwave Technol.*, Vol. 18, pp. 161-165, Feb. 2000.

[5] S. Hardrich, T. Schreiber, T. Pertsch, J. Limpert, T. Peschel, R. Eberhardt, and A. Tunnermann, "Thermo-optical behavior of rare-earth-doped low-NA fibers in high power operation," *Opt. Express*, Vol. 14, pp. 6091-6097, Jun. 2006.

[6] M. Sabaeian, H. Nadgaran, M. De Sario, L. Mescia, and F. Prudenzano, "Thermal effects on double clad octagonal Yb:Glass fiber laser," *Opt. Mat.*, Vol. 31, pp. 1300-1305, 2009.

[7] L. Li, H. Li, T. Qui, V.L. Temyanko, A. Schulzgen, A. Mafi, J. V. Moloney, and N. Peyghambarian, "3-Dimensional thermal analysis and active cooling system of short-length high-power fiber lasers," *Opt. Express*, Vol. 13, pp. 3420-3428, May 2005.

[8] J. Limpert, T. Schreiber, A. Liem, S. Nolte, H. Zellmer, T. Peschel ,V. Guyenot, and A. Tunnermann, "Thermo-optical properties of air-clad photonic crystal fiber lasers in high power operation," *Opt. Express*, Vol. 11, pp. 2982-2990, Nov. 2003.

[9] D. Brown and H. J. Hoffman, "Thermal, Stress, and Thermo-optic Effects in High Average Power Double-Clad Silica Fiber Lasers," *IEEE J. Quantum Electron.*, Vol. 37, pp. 207-217, Feb. 2001.

[10] H. Nadgaran and P. Elahi, "The analytical investigation of the super-Gaussian pump source on the thermal, stress and thermo-optics properties of double-clad Yb:glass fiber lasers," *Pramana J. Phys.*, Vol. 65, pp. 95-105, Jul. 2005.

[11] T. Schreiber, F. Roser, O. Schmidt, J. Limpert, R. Iliew, F. Lederer, A. Petersson, C. Jacobsen, K. P. Hansen, J. Broeng, and A. Tunnermann, "Stress-induced single-polarization single-transverse mode photonic crystal fiber with low nonlinearity," *Opt. Express*, Vol. 13, pp. 7621- 7630, Sep. 2005.

[12] P. Li, Ch. Zhu, Sh. Zou, H. Zhao, D. Jiang, G. Li, and M. Chen, "Theoretical and experimental investigation of thermal effects in a high power Yb^{+3}–doped double-clad fiber laser," *Optics & Laser Technol.*, Vol. 40, pp. 360-364, 2008.

[13] J. Limpert, A. Liem, H. Zellmer, and A. Tünnermann, "500 W continuous-wave fiber laser with excellent beam quality," *Electron. Lett*., Vol. 39, pp. 645-647, Apr. 2003.

[14] Z. Ma, D. Li, J. Gao, N. Wu, and K. Du, "Thermal effects of the diode pumped Nd:YVO_4 slab," *Opt. Common*., Vol. 275, pp. 179-185, Mar. 2007.

[15] S. P. Timoshenko and J. N. Goodier, *Theory of Elasticity*, 3rd ed., New York: McGraw-Hill, 1984.

[16] W. Xie, S. C. Tam, Y. L. Lam, K. S. Lai, R. Wu, Y. L. Lim, and E. Lau, "Analysis of a dynamical procedure on diode-end-pumped solid-state lasers," *IEEE Quantum Electron.*, Vol. 37, pp. 1368-1372, Oct. 2001.